Polymer 49 (2008) 4188–4195

Contents lists available at ScienceDirect

Polymer

journal homepage: www.elsevier.com/locate/polymer

Scaling laws and internal structure for characterizing electrospun poly[(*R*)-3-hydroxybutyrate] fibers

Chi Wang*, Chia-Hung Hsu, I.-Hwe Hwang

Department of Chemical Engineering, National Cheng Kung University, Tainan 701, Taiwan, ROC

ARTICLE INFO

Article history:
Received 29 March 2008
Received in revised form 7 July 2008
Accepted 19 July 2008
Available online 25 July 2008

Keywords:
Poly[(*R*)-3-hydroxybutyrate] fiber
Electrospinning
Solution rheology

ABSTRACT

Using chloroform/dimethylformamide (CF/DMF) co-solvent, electrospinning of poly[(*R*)-3-hydroxybutyrate] (PHB) solutions was carried out at ambient temperature. The effects of the applied voltage (V), flow-rate (Q), and solution viscoelastic properties on the Taylor cone, electrified jet, and fiber morphology were investigated. In addition, the electric field developed by the needle-plate electrode configuration was calculated using a finite element analysis to reveal the tip-to-collector (H) effect. Among the processing parameters (V, Q and H), it was found that Q played a key role in determining the jet diameter (d_j) and electrospun fiber diameter (d_f), and scaling laws existed between them, i.e., d_j–$Q^{0.61}$ and d_f–$Q^{0.33}$. The diameter reduction ratios of D_o/d_j (D_o is the needle diameter) and d_j/d_f were measured as 50–120 and 5–10, respectively; it suggested that major jet stretching took place in the straight electrified jet region, and further chain orientation could be gained by the subsequent process of jet whipping. By changing PHB concentrations from 5 to 15 wt%, the solution viscosity (η_o) was increased from 100 to 4900 cP, whereas the surface tension and solution conductivity remained unchanged; it provided a good model solution to exclusively reveal the η_o effect on the electrospinning process. Our results showed that the η_o-dependence of d_j and d_f also followed simple scaling laws: d_j–$\eta_o^{0.06}$, and d_f–$\eta_o^{0.39}$, with a prefactor depending on the processing variables, mainly the flow-rate. Regardless of the PHB concentrations used, the obtained PHB fibers showed a similar crystallinity fraction of ca. 0.63 and possession of major α-crystals together with a small amount of β-crystals with zigzag chain conformation.

1. Introduction

Recently much attention has been paid to the development of biomaterials, such as ploy(lactic acid) and poly[(*R*)-3-hydroxybutyrate] (PHB), because of their environmental-friendly nature. Of significant importance are their applications in the tissue scaffolds owing to their specific biocompatible and biodegradable behaviors. Electrospinning is a powerful processing technique to prepare fiber mats with a controllable fiber diameter, thereby their pore sizes between entangled fibers. Electrospun fibers with a diameter ranging from 10 to 1000 nm could be readily obtained by selecting appropriate processing parameters. After revisiting this process by Reneker's group in the early 1990s, many researchers have been involved in this interdisciplinary field and tremendous electrospinning results have been presented in recent years [1–6]. However, because quite a few influential factors are mutually involved in the process, it becomes extremely difficult, if not impossible, to separate the individual influence on the process development. In some cases, controversial results have been reported in the literature owing to the differences in the experimental setup and misleading comparison of inconsistent bases.

Much of the electrospinning is performed using the needle as the capillary for solution protrusion and a conductive plate grounded as a collector for the electrospun fibers [7–9]. It should be remarked that indeed the electric field developed in this needle-plate (or line-plate) electrode configuration is highly non-uniform in the space intended for electrospinning; our previous study [10] showed that field strength concentrates at the needle-end, and decays in a power law manner with an exponent of ca. −1.21. The level of jet whipping in the "bending instability region" is dependent upon the electric field that the electrified jet experiences, i.e., the shorter the straight jet beneath the Taylor cone, the higher the electric field that a whipping jet will experience. Thus, a thorough understanding of the electric field distribution becomes inevitable to unveil the correlation between the electrified jets and electrospun fibers, suggesting further that it is of significance to study the effects of processing variables on the morphologies of the free cone/jet surface.

* Corresponding author. Tel.: +886 6 2757575x62645; fax: +886 6 2344496.
E-mail address: chiwang@mail.ncku.edu.tw (C. Wang).

0032-3861/$ – see front matter © 2008 Elsevier Ltd. All rights reserved.
doi:10.1016/j.polymer.2008.07.033

Nomenclature

c^*	overlapping concentration (–)
c_e	entanglement concentration (–)
d_j	diameter of straight jet end (μm)
d_f	diameter of electrospun fiber (μm)
D_o	outer diameter of needle (mm)
De	Deborah number (–)
E_o	nominal electric field (=V/H, kV/m)
E_j	electric field at the straight jet end, determined by finite element analysis (kV/m)
G'	dynamic storage modulus (Pa)
G''	dynamic loss modulus (Pa)
H	tip-to-collector (working) distance (cm)
H_c	cone height, measured from the needle-end to the apex of Taylor cone (mm)
l_j	length of the straight jet (mm)
L_j	distance from the needle-end to the straight jet end (=$H_c + l_j$, mm)
Q	solution volume flow-rate (mL/h)
v_j	jet velocity at the straight jet end (m/s)
V	applied voltage (kV)
V_s	lower bound voltage for the cone-jet electrospinning mode (kV)
V_{us}	upper bound voltage for the cone-jet electrospinning mode (kV)
T_m	melting temperature of PHB (°C)
η_o	zero shear viscosity of solution (cP)
η^*	complex viscosity of solution (cP)
κ	solution conductivity (μS/cm)
γ	surface tension (dyne/cm)
ρ	density (g/cm^3)
ϕ_v	volume fraction of polymers (–)
ϕ^{DSC}	fiber crystallinity measured by DSC (–)
ε	relative permittivity (–)
ω	frequency (rad/s)
J_s^o	recoverable shear compliance (Pa^{-1})
τ_o	relaxation time (s)

Solution electrospinning of PHB [11–13] and its copolymers with hydroxyvalerate (PHBV) [14,15] or hydroxyhexanoate (PHBHHx) [16] has been investigated previously in an attempt to obtain thinner fibers than that prepared by the melt-spinning process [17–19]. By melt-spinning, the diameter of the as-spun PHB fibers is typically 200–300 μm, and the fiber crystallinity is rather low owing to its slow crystallization character. Thus, annealing of the melt-spun fibers under tension above its glass transition temperature is generally required to obtain PHB fibers with sufficient mechanical strength for practical applications. Depending upon the post-spun treatments, drawing and annealing procedures lead to the development of higher order structure, e.g., the coexistence of stable α-form and the metastable β-form crystals [17–19]. In this paper, electrospinning of well-characterized PHB solutions was performed at ambient temperature. The effects of applied voltage and flow-rate on the cone/jet/fiber morphologies were experimentally investigated. By means of finite element analyses, a theoretical calculation was carried out to determine the electric field distribution setup by the needle-plate configuration, which was used to elucidate the effect of tip-to-collector distance and the level of jet whipping. By fixing all the processing parameters except the solution viscosity, the scaling laws between the jet/fiber diameter and solution viscosity were derived, and the results were compared with those reported previously. Finally, the internal structure of the electrospun PHB fibers was characterized by several analytical techniques to unveil processing effects and compare with those prepared from the melt-spinning process.

2. Experimental

2.1. Materials and solution characteristics

PHB powder samples were purchased from Sigma–Aldrich, and chloroform (CF) and dimethylformamide (DMF) were used to prepare the electrospinning solutions. The solubility parameters (δ) for the CF, DMF, and PHB [20] were reported to be 9.3, 12.1 and 9.7 (cal/cm^3)$^{0.5}$. Using an Ubbelohde capillary viscometer, the intrinsic viscosity, [η], of the PHB/CF solutions was determined to be 2.136 dL/g, which gave an average molecular weight of 262.1 kg/mol on the basis of the Mark–Houwink–Sakurada equation with the reported values of K (=7.7×10^{-5}) and a (=0.82) [21]. Solutions were prepared on a weight basis, and the volume fraction of polymer (ϕ_v) was calculated from the pure component densities ($\rho_{CF} = 1.480$, $\rho_{DMF} = 0.944$, and $\rho_{PHB} = 1.230$ g/cm^3) assuming negligible volume change on mixing.

Properties of the electrospinning solutions, i.e., conductivity (κ), surface tension (γ), and viscosity (η_o) were measured at room temperature. Surface tension and conductivity of the prepared solutions were measured using Face surface tension meter (CBVP-A3) and Consort conductivity meter (C832), respectively. Linear viscoelastic properties of the solutions were measured in a Rheometrics (ARES) using a cup-and-bob feature. Oscillatory shear mode was used to determine the storage modulus $G'(\omega)$ and loss modulus $G''(\omega)$ over a range of frequencies. Zero shear viscosity η_o was determined from the loss modulus data at low frequencies: $\eta_o = \lim_{\omega\to 0} G''(\omega)/\omega$. Recoverable shear compliance J_s^o was determined from the storage modulus data at low frequencies: $J_s^o = 1/\eta_o^2 \lim_{\omega\to 0} G'(\omega)/\omega^2$. The relaxation time τ_o was estimated by $\tau_o = \eta_o J_s^o$ [22]. The charge relaxation time τ_c was calculated by a simple relation: $\varepsilon/(4\pi\kappa)$, where ε was the solution permittivity; ε was mainly related to the solvent used and assumed to be relatively independent of the polymer concentration [23].

2.2. Processing and measurements

To prevent the cone from clogging as a result of the high volatility of CF, a jacket was constructed to introduce saturated chloroform to blanket the Taylor cone by using N_2 as a carrier gas [24]. The homogeneous polymer solution was delivered by a syringe pump (Cole-Parmer) at a controlled flow-rate (Q, ranging from 0.5 to 35 mL/h) to the needle (i.d./o.d./length = 1.07/1.47/40.0 mm) where an electrical voltage (V, ranging from 5 to 30 kV) was applied by a high-voltage source (Bertan, 205B). To construct a line-plate electrode configuration, a steel net (30×30 cm^2) was used as a collector for the electrospun fibers at a tip-to-collector distance (H) of 14 cm below the needle tip. Thus, the nominal electric field strength was expressed by $E_o = V/H$. Four CCDs were used to observe the morphologies of the electrified cone and jet during electrospinning, i.e., (1) the cone height, H_c, defined by the distance from the needle-end to the Taylor-cone apex, (2) the straight jet length, l_j, measured from the Taylor-cone apex to the terminal jet, where jet whipping was initiated, (3) the terminal jet diameter, d_j, determined by a laser diffraction technique, and (4) the jet whipping behavior observed by a high-speed camera (Redlake, Motion Pro 10000) to capture images at a frame rate of 10^4 frame/s. The details have been described previously [25]. The fiber morphology was observed using scanning electron microscope (SEM, Hitachi S4100) and fiber diameters were measured within electron micrographs from a population of ~500 fibers, from which the average fiber diameter (d_f) and the corresponding standard error were determined. To characterize the internal structure of

electrospun fibers, wide-angle X-ray diffraction (WAXD) patterns and FTIR spectra were obtained using a Dmax2000 X-ray goniometer (Rigaku, Cu target) and Spectrum 100 (Perkin–Elmer Co.), respectively. IR absorption peaks at 1721 cm^{-1} and 1735/1745 cm^{-1} were assigned to the C=O stretch band in the crystalline and amorphous phases, respectively [19,26]. The area of absorbance peak at 1453 cm^{-1} (A_{1453}) could be used as an internal standard for thickness correction [27]. After curve de-convolution in the 1650–1800 cm^{-1} region, the area of the absorbance peak at 1721 cm^{-1} (A_{1721}) was obtained, and the relative crystallinity of PHB fibers was estimated by the A_{1721}/A_{1453} ratio. In addition, the single absorbance peak at 1228 cm^{-1} was also attributed to the crystalline phase [27] and the A_{1228}/A_{1453} ratio was determined to provide the relative crystallinity as well. Thermal properties were analyzed using a Perkin–Elmer differential scanning calorimeter (DSC7) at a heating rate of 10 °C/min under nitrogen. The melting point and melting enthalpy were determined from the peak temperature and the area under the melting peak. Then, the crystallinity fraction (ϕ^{DSC}) of the electrospun fibers was determined from the melting enthalpy to the one with pure α-form crystals (146 J/g) [28].

2.3. Electric field simulation

Using the FLUX2D®9.10 software, the electric field strength from the needle-end to the grounded collector was calculated through a finite element analysis. Owing to the axisymmetric geometry, only half space with respect to the needle axis was necessarily considered to construct for the 3-D electrostatics problem. The geometry used in the electrospinning experiments was adopted to calculate the electric field setup by the needle-plate configuration without considering the electrified fluid effects. Fine element meshes were built near the needle-end corner because of the presence of electric field concentration, and coarse element meshes were used for the far field space. At least 20 elements right beneath the needle-end were constructed for a precise calculation. Within the domain of interest, ca. 6000 triangle elements were used for the finite element analysis. The relative permittivity of the air was assumed to be 1.0. After the potential on the needle surface and the grounded plate were specified, the potential in the desired domains was calculated by solving the Poisson equation. Then, the electric field (E) determined from the gradient of simulated potentials was calculated to obtain the electric field distribution along the z direction from the needle-end ($z=0$) to the grounded plate ($z=H$).

3. Results and discussion

3.1. Solution properties

Once the frequency dependences of G' and G'' are measured for various solutions, the complex viscosity (η^*) versus angular frequency (ω) is determined and shown in Fig. 1, which overlaps with the viscosity obtained from the steady shear measurements (not shown), thereby validating the Cox–Merz rule for the PHB solutions. For low concentrations the solutions exhibit a Newtonian behavior, but increasing the PHB concentration leads to the shear thinning behavior at high ω, i.e., η^*–ω^{-n} with the power law index n increasing with the PHB concentration; being 0.22 for the 9 wt.% and 0.36 for the 16 wt.% solution. The zero shear viscosity (η_o) and J_s^o are shown in Fig. 2, together with the calculated τ_o. The log–log plot shows that η_o is increased with increasing PHB content, and a constant slope of 3.64 is reached at a concentration of 4 wt.% (5.0 vol.%) for the PHB/CF solution. It suggested that a semi-dilute regime with entangled PHB chains is reached for solutions possessing a concentration above this critical value (c_e) [29,30]. The overlapping concentration, c^*, was estimated by the reciprocal of the $[\eta]$ to be 0.32 wt.% (0.38 vol.%), leading to the c_e/c^* ratio of ~13.

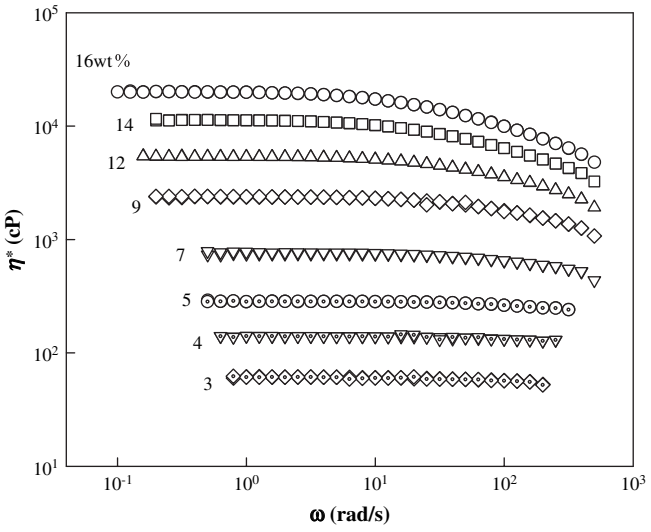

Fig. 1. Double logarithmic plots of complex viscosity, η^*, versus frequency, ω, for PHB/CF solutions with various concentrations.

Previous studies have already shown that electrospinnability of polymer solutions is mainly determined by the dielectric constant of the solvent used; a solvent with a larger dielectric essentially produces smaller diameter-scale fibers [31]. CF solvent has a lower dielectric constant (~4.8) and conductivity (<0.1 μS/cm) in comparison with that of DMF solvent (36.7 and 0.6 μS/cm, respectively). To enhance the solution properties, DMF was added to form a CF/DMF co-solvent of 9/1 weight ratio, which was used to prepare the solutions for electrospinning. After DMF molecules were dissolved, the PHB chain conformation in the solution might change because of the variation of the solvent/polymer affinity. As shown in Fig. 2, the critical concentration for the development of entangled solution is increased to 5 wt.% (5.9 vol.%) but the terminal slope remains slightly unchanged (~3.60). Owing to the poor affinity of DMF to the PHB chains, moreover, η_o is reduced at a fixed PHB concentration, which favors the formation of thinner PHB fibers. Similar solvent-quality dependence of η_o has been reported for PMMA solutions using co-solvents of CF/DMF with various compositions [32]. According to Fig. 2(b), J_s^o is decreased with PHB content (ϕ_v); whereas τ_o is increased with ϕ_v; both rheological quantities follow a power law relation expressed by J_s^o–$\phi_v^{-1.51}$ and τ_o–$\phi_v^{2.37}$. Depending on the concentration, the relaxation time of PHB solution ranges from 5 to 50 ms, which is comparable to the processing time normally observed during electrospinning.

The surface tension of the solution is independent of the polymer concentration, but is determined by the solvent used as shown in Fig. 3. For the CF/DMF = 9/1 co-solvent, the measured γ value was 28.4 dyne/cm, which was close to the one determined by its volume composition. Also given in Fig. 3 is the conductivity of various solutions prepared by CF/DMF co-solvent. It is seen that κ is increased with increasing PHB concentration and reaches a constant value of 2.53 μS/cm for the entangled solutions (5–13 wt.%). Based on the measured κ, the calculated τ_c is in the range of 13 ns, which is much lower than the processing time, ca. several ms. It indicates that the induced charge by the applied E field during electrospinning will migrate quickly to the cone/jet surface in most of the electrospinning cases [33]. For the PHB/CF solutions, however, κ was relatively low (<0.1 μS/cm) regardless of the polymer concentration.

Based on the above results, the application of CF/DMF = 9/1 co-solvent instead of using neat CF, will give rise to a PHB solution with a lower viscosity and enhanced conductivity; both effects favor the production of thinner fibers. It should also be noted that a small

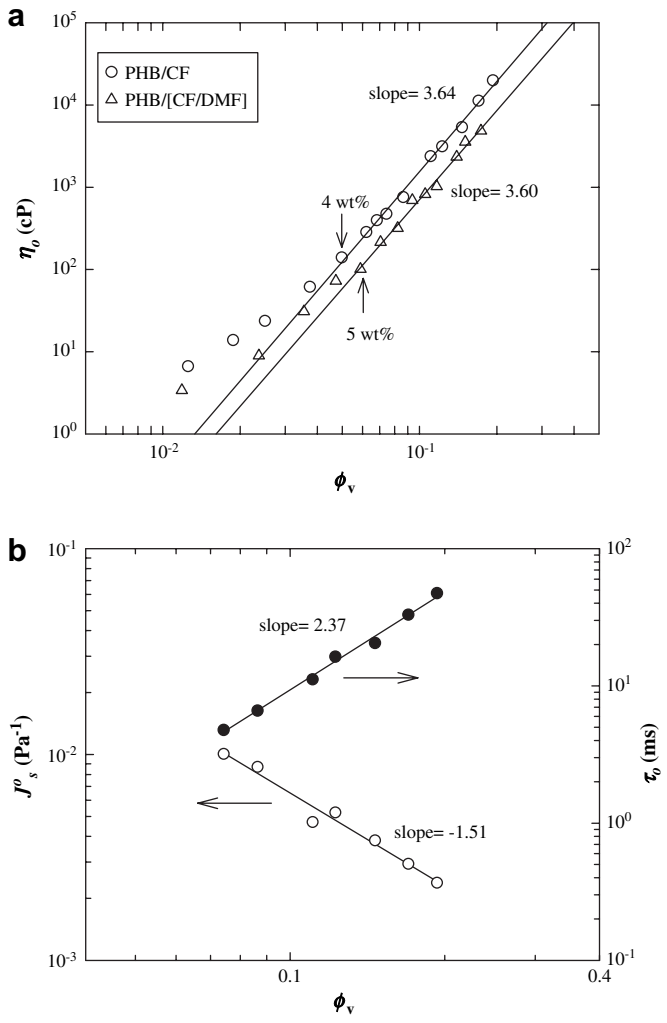

Fig. 2. (a) A plot of zero shear viscosity versus volume fraction of PHB. The deviation of the final straight line is indicated by the arrows, where the incipient concentration for the chain entanglement, c_e, is determined. (b) Volume-fraction dependence of recoverable shear compliance, J_s^o, and relaxation time, τ_o, of PHB/CF solutions.

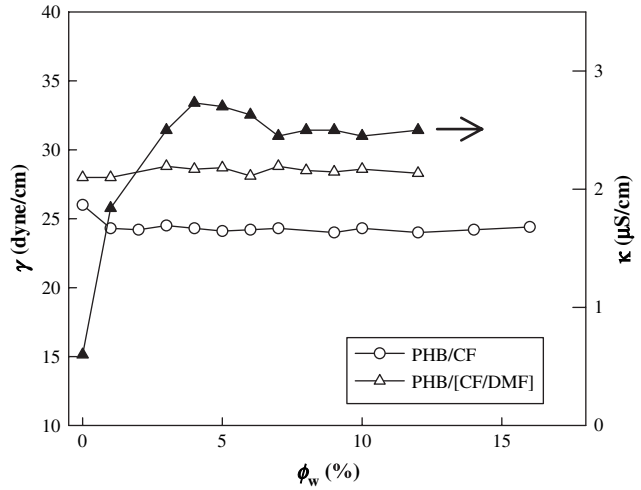

Fig. 3. Composition dependence of surface tension (open symbols) and conductivity (filled symbols) of PHB solutions.

increase in surface tension is seen, thereby possibly giving a negative effect on the fiber diameter.

3.2. Effects of H, V and Q on electrospinning of PHB/[CF/DMF] solutions

It is now well known that electrospinning will be degenerated into electrospraying and only particulates are produced when a solution in the unentangled regime is used. With increasing polymer concentration, fiber-like structure is initially observed for a solution with a concentration of c_e. However, if the entanglement network in the solution state is insufficiently strong to prevent the Raleigh (axisymmetric) instability, fibers with beads along the string (beaded fibers) will be yielded. To prepare uniform and bead-free fibers, a higher concentration (1.75–2.5 times of c_e) is essentially required for the electrospinning solution [34,35]. For the present PHB/[CF/DMF] system, however, it is of interest to notice that uniform PHB fibers can be deduced from the 5 wt.% solution, suggesting the integrity of the network structure developed at the concentration of c_e.

For a given solution, the search for the processing window is of importance in determining the appropriate processing variables of *Q*, *V*, and *H*. Fig. 4 shows the simulation results of the electric intensity (*E*) distribution along the needle axis from the needle-end ($z=0$) to the grounded collectors, and the *H* effect has been revealed by two typical values, i.e., 14 and 42 cm. The nominal value of E_o is given by *V*/*H*. Apparently, a significant intensity concentration is observed at the needle-end, and the magnitude of *E* is decreased with increasing distance, and follows a scaling law of E–$(z/D_o)^{-\alpha}$ with a derived α of 1.27 for $H=14$ cm and 1.31 for $H=42$ cm. Importantly, the electric field is found to be relatively unchanged in the z/D_o range of 0–30 in spite of the 3-time difference in the tip-to-collector distance. An increase in *H* merely results in the reduction of the electric intensity adjacent to the collector, being 6.0 kV/m for $H=14$ cm and 2.1 kV/m for $H=42$ cm. The *E* strength near the collecting plate is constant and its magnitude is about one-order lower than the nominal *E*. The results as shown in Fig. 4 suggest that *H* is not a crucial factor in the electrospinning process when a line-plate electrode configuration is adopted. However, a minimum *H* value is still required to allow the sufficient solvent evaporation occurring particularly in the "bending instability region" for preparing dry fibers electrospun on the collector.

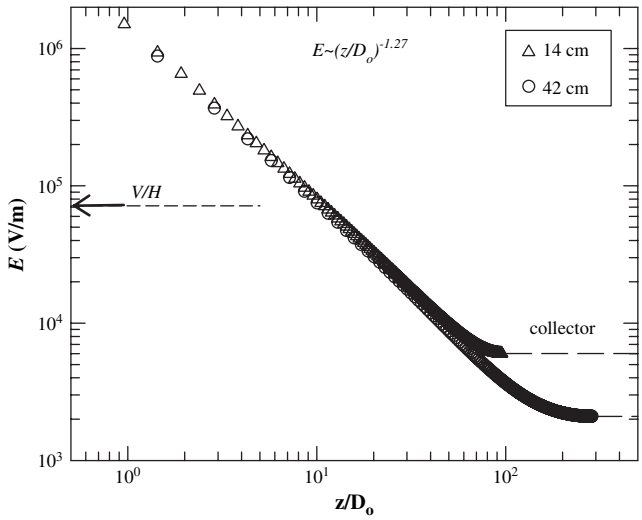

Fig. 4. Effects of *H* on the distribution of electric field from the needle-end ($z=0$) toward the grounded collector obtained from the FEA simulation. The diameters of needle and grounded collector are 1.47 and 600 mm, respectively. The needle length is 40 mm and the potential difference is 10 kV. The arrow indicates the nominal *E* for $H=14$ cm.

Based on our FEA calculations, we also found that the electric field is proportional to the applied voltage, i.e., the electric field is doubled when the applied V is 2 times larger. In addition, the geometry of the needle, such as needle length and diameter, also has impacts on the effective electric field. The details will be presented and discussed in our forthcoming article. For the needle-plate electrodes used for the present experiments, the electric field can be well described by E (in the unit of V/m) $= 146.05V^{1.0}$ $(z/D_o)^{-1.27}$ in the z/D_o range from 0.1 to 50. Judging from the above calculations, the determination of the electric intensity at which "jet whipping" takes place is of importance in predicting the fiber diameter since further jet stretching is associated with repulsive forces existing between the "bending and electrified" jets. When experiencing a higher E, the bending jet segment will be more effectively stretched (or whipped), thereby producing finer fibers after solvent evaporation.

For a given H, experimentally there is a close relation between the applied Q and V, as shown in Fig. 5, where three typical solutions are demonstrated to reveal their processing windows (functioning domains) [25,36]. The filled and open symbols represent, respectively, the minimum and maximum V (denoted by V_s and V_{us}, respectively) required for obtaining a stable cone-jet electrospinning mode, which readily generates reproducible fiber morphology. A voltage lower than V_s yields a dripping mode, whereas a voltage higher than V_{us} leads to the contraction of the Taylor cone inside the needle channel; both are not the desired electrospinning mode. Both V_s and V_{us} are found to increase with increasing Q and a scaling law is developed. The derived exponent for the V_{us}–Q relation is approximately unchanged, i.e., V_{us}–$Q^{0.25-0.29}$, regardless of the solution concentration. However, the exponent for the V_s–Q relation is gradually decreased from 0.25 for the 5 wt.% to 0.08 for the 15 wt.% solution. For a given Q, the voltage range available for the cone-jet electrospinning mode is increased for solutions with a higher PHB concentration. Moreover, a Q limitation also exists for processing; a too low Q will result in the insufficient solution supply to the Taylor cone, and a too high Q causes the inapplicability of high V applied; both lead to an unstable electrospinning mode.

To reveal the effects of Q and V, the 11 wt.% solution was electrospun with a constant H of 14 cm for electrospinning. According to the processing window shown in Fig. 5, the available V range for a given Q of 5 mL/h is 7.5–12 kV; whereas the Q range available for a fixed V of 10 kV is 3–24 mL/h. The effects of V and Q on the cone height (H_c), position of the straight jet end ($L_j = H_c + l_j$), jet diameter (d_j) and the fiber diameter (d_f) are displayed in Table 1, together with the terminal jet velocity ($v_j = 4Q/(\pi d_j^2)$) and the drawability of the whipping jet estimated by $\phi_v(d_j/d_f)^2$ [10,25]. Also shown in Table 1 is the calculated electric strength (E_j) at the location where the jet whipping is initiated ($z = L_j$). For a fixed Q, the application of a larger V leads to a smaller Taylor cone and longer straight jet with a smaller jet diameter. For electrospinning a 6 wt.% polyethylene oxide/water solution [37], a longer straight jet was also observed under a larger V applied owing to the possession of higher initial stress in the cone-jet entrance zone, which stabilized the straight jet for a longer distance. Although the E field is increased with applied V, as mentioned previously, the calculated E_j is similar (28.8–34.7 kV/m) in all the cases owing to the possession of a larger L_j when a higher V is used. The magnitude of E_j is lower than the nominal electric field (53.6–85.7 kV/m) determined by V/H. Moreover, electrospun fibers with a smaller diameter are obtained when a higher V is applied. The traveling time of fluid elements in the straight jet region was estimated by l_j/v_j to be 1.8–2.8 ms, which was reasonably acceptable to support the assumption of limited solvent evaporation prior to jet whipping. Nevertheless, slight concentration variation might be inevitable along the straight jet if a volatile solvent is used. As shown in Fig. 2b, the relaxation time of PHB chains in the CF solvent is ca. 5–50 ms, mainly depending upon the PHB concentration. Provided that τ_o is assumed unchanged in the CF/DMF solvent (18.8 ms for the 11 wt% solution), the Deborah number (De) was estimated by a simple expression of $De = \tau_o/(l_j/v_j)$ to be 6.7–10.4, suggesting that elastic deformation of PHB chains dominates in the straight jet flow region. In other words, effective chain stretching essentially occurs and chain orientation prevails for a fluid element flowing from the Taylor cone to the convergent jet channel. Our calculated v_j is increased with increasing V; this finding is consistent with previous report by using a laser Doppler velocimeter for the v_j measurements [37]. In contrast with the theoretical calculation by Yarin et al. who showed a significant draw ratio of $\sim 10^4$ during jet whipping process [38], it should be remarked that our calculated drawability of whipping jet is much lower and is in the range of 2–25, depending upon the electrospinning conditions and solutions used (Tables 1 and 2). This discrepancy implies that significant solvent evaporation takes place right after the electrified jet entering the "jet whipping envelope" and more detailed solvent/solute information, i.e., evaporation mechanism and concentration/temperature dependence of material properties, is needed for a better result of theoretical modeling [38]. It should be noted, however, that a severe limitation on the applied V range (7.5–12.0 kV) is frequently encountered, leading to an uncertainty in *quantitatively* determining the V-dependence of the cone/jet/fiber morphologies. In contrast, ca. 8 times difference

Table 1
Effects of applied voltage and flow-rate on the morphologies of the electrified cone and jet as well as the electrospun fibers

Voltage (kV)	Q (mL/h)	H_c/D_o	L_j/D_o	E_j (kV/m)	d_j (μm)	d_f (μm)	Drawability	v_j (m/s)
7.5	5	1.52	17.2	29.5	14.74 ± 1.02	3.21 ± 0.41	2.70	8.1
8.5	5	1.08	18.0	31.6	14.00 ± 0.37	3.08 ± 0.27	2.64	9.0
10	5	0.62	19.0	34.7	12.61 ± 0.22	2.90 ± 0.37	2.42	11.1
11	5	0.44	22.2	31.3	12.03 ± 0.26	2.59 ± 0.29	2.76	12.2
12	5	0.28	25.4	28.8	11.34 ± 0.31	2.40 ± 0.42	2.85	13.8
10	3	0.24	18.8	35.2	11.06 ± 0.30	2.32 ± 0.23	2.91	8.7
10	10	1.10	18.2	36.7	19.92 ± 0.76	3.49 ± 0.46	4.17	8.9
10	20	2.94	19.2	34.2	32.22 ± 1.90	4.19 ± 0.71	7.57	6.8
10	24	4.10	18.8	35.2	37.87 ± 2.06	4.83 ± 0.82	7.87	5.9

11 wt% PHB/[CF/DMF] solutions and $H = 14$ cm.

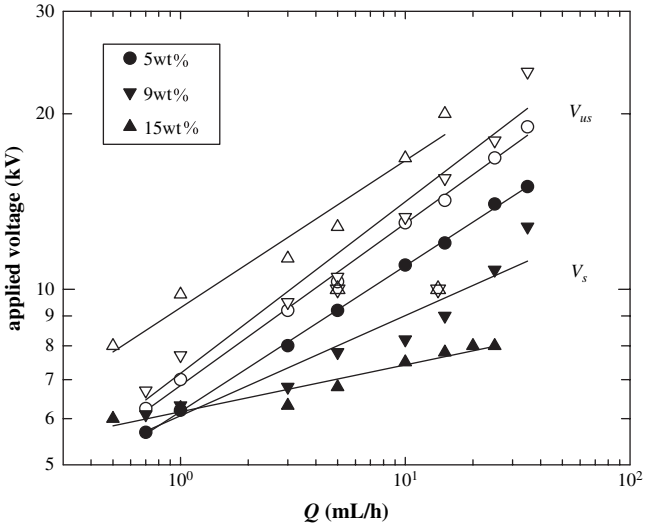

Fig. 5. Composition dependence of functioning domains for the PHB/[CF/DMF] solutions at a given tip-to-collector distance of 14 cm. The filled and open symbols denote the lower (V_s) and upper (V_{us}) bound voltage, respectively, for a stable cone-jet electrospinning mode.

Table 2
Effects of solution viscosity on the morphologies of the electrified cone and jet as well as the electrospun fibers

Group	wt (%)	η_o (cP)	H_c/D_o	L_j/D_o	E_j (kV/m)	d_j (μm)	d_f (μm)	Drawability	v_j (m/s)
I	5	101	0.32	11.8	63.6	12.14 ± 0.36	0.96 ± 0.28	20.48	12.0
	7	319	0.38	12.6	58.5	12.33 ± 0.18	1.61 ± 0.23	7.51	11.6
	9	823	0.52	18.2	36.7	12.43 ± 0.09	2.33 ± 0.28	3.64	11.5
	11	1670	0.62	19.0	34.7	12.61 ± 0.22	2.90 ± 0.37	2.42	11.1
	15	4869	0.88	26.0	23.3	14.69 ± 0.31	3.88 ± 0.48	1.83	8.2
II	6	214	1.16	6.0	150.1	23.42 ± 0.46	1.80 ± 0.38	25.54	9.0
	8	695	1.30	11.4	66.4	26.18 ± 0.28	2.74 ± 0.63	10.65	7.2
	10	1023	1.70	12.6	58.5	27.66 ± 0.33	3.61 ± 0.47	5.50	6.5
	13	3550	2.74	21.4	29.8	28.83 ± 0.45	5.67 ± 1.39	1.82	6.0

The flow-rates used are 5 and 14 mL/h for groups I and II, respectively, whereas the voltage and H are fixed at 10 kV and 14 cm.

in the available Q can be applied for a fixed V to study the Q-dependence of the free liquid jet and fiber morphologies, as shown in Table 1 as well.

With increasing Q, the Taylor cone is bigger but the straight jet length is shortened; both effects result in a constant L_j for the whipping jet experiencing a similar E_j of ~35 kV/m. Moreover, both d_j and d_f become larger. Of particular interest is a simple scaling law observed for the d_j–Q relation: d_j–$Q^{0.61}$, implying that Q is the most important processing variable, instead of V and H, to manipulate the free jet diameter. By means of a theoretical consideration, Gañán-Calvo has derived an empirical relation for the Q-dependence of jet diameter, i.e., d_j–$Q^{0.5}$ [39]. A similar exponent and consistent results have also been found on electrospinning of PS solutions with different solvents [25].

For a given solution, the final fiber diameter is crucially determined by two measured quantities: the first is the d_j, and the second is the E_j, which the whipping jet experienced at L_j. Under an enhanced E_j, the whipping process will be more effective to further reduce the jet diameter owing to the electric repulsion between liquid segments of the whipping jet. Thus, a straight jet with a shorter length and smaller d_j is believed to yield electrospun fibers with a smaller diameter. In essence, there an intimate correlation between d_j and d_f should exist. Owing to the coupled effects of solvent evaporation and jet whipping, theoretical derivation essentially becomes rather difficult, if not impossible, to carry out in determining the d_j–d_f relation. Here, we tentatively attempt to construct the log–log plot of measured d_f versus d_j to reveal the possible relation. As shown in Fig. 6, for a given electrospinning solution a master curve is obtained by an expression of d_f–$d_j^{0.54}$, regardless of the processing variables used. For PS solutions with various solvents used, a similar exponent (~0.50) has been reported previously [25]. Provided that jet stretching could be negligible (or absent) during the whipping process, a simple relation was readily derived to be [40]: $d_f = \phi_v^{0.5} d_j^{1.0}$ for simply considering the solid content conservation. Our derived exponent, ~0.54, suggested that jet stretching associated with the whipping process should not be neglected in determining the final value of d_f, and the level of jet stretching could be estimated by the calculated drawability (Table 1).

3.3. Viscosity dependence of jet/fiber morphologies

All the previous electrospinning results have demonstrated that viscosity is the most important solution property among all in determining the fiber diameter. To vary the viscosity by changing the polymer concentration, the surface tension and conductivity might also be altered in some systems, thereby producing a combinational effect and plausibly a misleading conclusion. For the present solution studied, both γ and κ remain unchanged, but

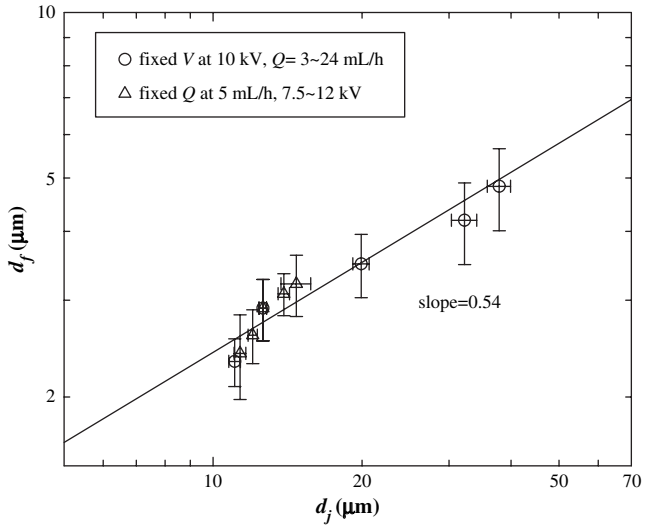

Fig. 6. A plot of fiber diameter versus jet diameter obtained from electrospinning of the 11 wt.% PHB/[CF/DMF] solution under different Q and V. H is fixed at 14 cm.

η_o increases significantly with PHB concentration for an entangled solution, as shown in Figs. 2a and 3. Thus, the exclusive effects of η_o on the cone/jet/fiber morphologies are deduced by simply changing the PHB concentration and the results are displayed in Table 2. To further explore the Q effect, the entangled solutions with a concentration range of 5–13 wt% are separated into two groups: one is performed using a given Q of 5 mL/h, the other of 14 mL/h. Based on the processing window shown in Fig. 5, the magnitudes of V and H can be controlled to be constant for both groups at 10 kV and 14 cm, respectively (as shown by the asterisk symbols).

As the η_o of the electrospinning solution is increased, H_c, L_j and d_j all become larger, but the corresponding E_j is obviously decreased. As expected, fibers with a larger diameter are produced from a more concentrated solution, which yields a fatter straight jet with a longer length experiencing a lower electric field for the whipping process. Both groups show a similar trend. Fig. 7 shows the double logarithm plots of d_j and d_f versus η_o, from which two scaling laws are derived: $d_j = m\eta_o^{0.04-0.07}$ and $d_f = n\eta_o^{0.36-0.41}$ with the pre-factors of m and n depending upon the Q applied. A higher Q gives larger values of m and n. According to the derived exponents, a weak η_o-dependence of d_j, but a strong η_o-dependence of d_f is obtained, suggesting lower drawability in the jet whipping process for the more concentrated solution resulting from both higher viscosity, as well as longer straight jet. The present exponents derived are in agreement with those obtained from the electrospinning of PS/THF solutions [25] with controlled κ (=1.15 μS/cm) and γ (=24.2 dyne/cm), whose data are also included in Fig. 7 as the broken lines for comparison. The processing variables for the PS solutions were $Q = 3$ mL/h, $H = 14$ cm and 10 kV, and similar magnitudes of E_j were obtained. At a given η_o, the jet diameter of PS solution is smaller, but fatter PS fibers are obtained in comparison with those of PHB counterparts. The calculated drawability of whipping PS jet (0.6–2.2, [25]) is apparently lower that that of the PHB jet. The small-diameter PS jet could be attributed to a low Q applied. However, owing to the more volatile nature of THF in contrast with the DMF/CF co-solvent used for PHB polymers, severe stretching of PS jets prior to polymer solidification is hindered, and large-diameter PS fibers are produced.

In studying the electrospinnability of polyacrylonitrile/DMF solutions [10], we also obtained similar scaling laws (d_j–$\eta_o^{0.08}$, d_f–$\eta_o^{0.52}$) for solutions with a η_o range of 170–2750 cP in spite of the fact that γ was kept constant at 36.3 dyne/cm, but k was increased from 36.0 to 51.5 μS/cm as the PAN concentration was increased. In

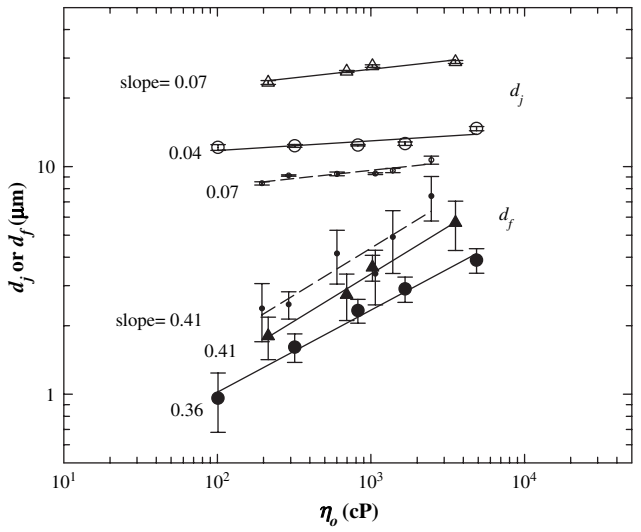

Fig. 7. Viscosity dependence of jet diameter (d_j, open symbols) and fiber diameter (d_f, filled symbols) for the PHB/[CF/DMF] solutions electrospun at ambient temperature. For all the solutions, the surface tension and conductivity are the same: $\gamma = 28.4 \pm 0.3$ dyne/cm, $\kappa = 2.53 \pm 0.10$ μS/cm. Key: (○) 5, 7, 9, 11 and 15 wt% solutions electrospun at $Q = 5$ mL/h; (△) 6, 8, 10 and 13 wt% solutions electrospun at $Q = 14$ mL/h. The broken lines are results by electrospinning PS/THF solutions taken from Ref. [25]. All the data shown are obtained under the processing condition of $H = 14$ cm and 10 kV.

contrast, a larger exponent for the η_o-dependence of d_f has been reported for electrospinning of poly(methyl methacrylate)/DMF solutions (~0.71) by Gupta et al. [41], and poly(ethylene terephthalate-*co*-ethylene isophthalate)/(CF/DMF) solutions (~0.8) by McKee et al. [34]. However, a lower exponent (~0.16) was found for electrospinning of the poly(ethylene oxide)/water solutions by Daga et al. [42].

3.4. Internal structure of the electrospun PHB fibers

In the electrospinning of PHB/CF solutions, smoothness of the as-spun PHB fibers was closely related with the environmental humidity for electrospinning; a humidity of above 50% usually leads to the presence of pore structure on the surface. Although the Taylor cone was purged with N_2 to prevent its blockage leading to the unstable spinning, the "jet whipping region" was not blanketed by the N_2 atmosphere. Similar pore dimensions have been observed in electrospinning of PS/THF solutions [9,25]. Casper et al. suggested that the porous surface of electrospun fibers is attributed to a combination of both "breath figure" formation and thermally (and vapor) induced phase separation [9]. A recent paper by Dayal et al. [43] provided a theoretical foundation to support the argument of phase separation. Using the CF/DMF co-solvent instead, it was found that the pore structure could be greatly eliminated owing to its reduced volatility, and even be prevented under appropriate conditions. However, the collected PHB fibers possessed a small amount of DMF, as evidenced by FTIR with a small absorbance peak at 1673 cm^{-1}. The residual DMF solvents are likely to be constrained in the skin region of the fibers in consideration of evaporation mechanism during the high frequency of jet whipping. Indeed, it was further evidenced by the "surface necking" phenomenon when the as-spun fibers were under a small tensile strain. In turn, the plasticized skin region will facilitate the production of thinner PHB fibers with a more uniform internal structure by further stretching provided that a rotating drum with a linear velocity higher than that of the flying jets is used as the collector. On the other hand, by electrospinning the whipping jet directly into the water bath as a grounded collector, FTIR measurements on the post-dried fibers at 45 °C showed no trace of DMF left. It is also worth mentioning that, by controlling the spinning circumstances, connecting of jet segments during the whipping process is frequently observed by using a high-speed camera; this essentially produces collected fiber mats with a better integrity. The coalescence of PHB fibers at their contact points was also reported by Ishii et al. [12] In addition, similar jet emergence during whipping was also observed by Reneker et al. [44] in electrospinning of polycaprolactone/acetone solutions. Based on our measurements, the flight speed of the whipping dried fibers toward the collector is in the range of 1.05–1.23 m/s, which is considerably lower than the terminal jet velocity (Tables 1 and 2), plausibly owing to the presence of a lower electric field for a distance far from the needle tip (Fig. 4).

The WAXD profiles of the collected fibers electrospun from various solutions are shown in Fig. 8, together with that of the PHB powder sample. In addition to the presence of orthorhombic α-form crystals with helical chain conformation [45], the electrospun PHB fibers also possess a small amount of β-form crystals with zigzag conformation as revealed by the diffraction hump located at 2θ of 19.95° [46]. Using a low conductivity solvent of hexafluoro-2-propanol ($\varepsilon = 16.8$), Ishii et al. [12] also reported the possession of β-form crystals in their PHB (720 kg/mol) fibers electrospun from solutions with a concentration lower than 1 wt%. The presence of β-form crystals indicates a high level of molecular stretching in the amorphous region between the α-crystalline lamellae, which might develop first [12]. As mentioned previously [25], significant chain orientation of the PHB molecules is likely to take place in the entrance region from the Taylor cone to the ejecting jet, where a severe jet stretching is induced by the convergent flow and electric repulsion. The orientation-induced crystallization of the

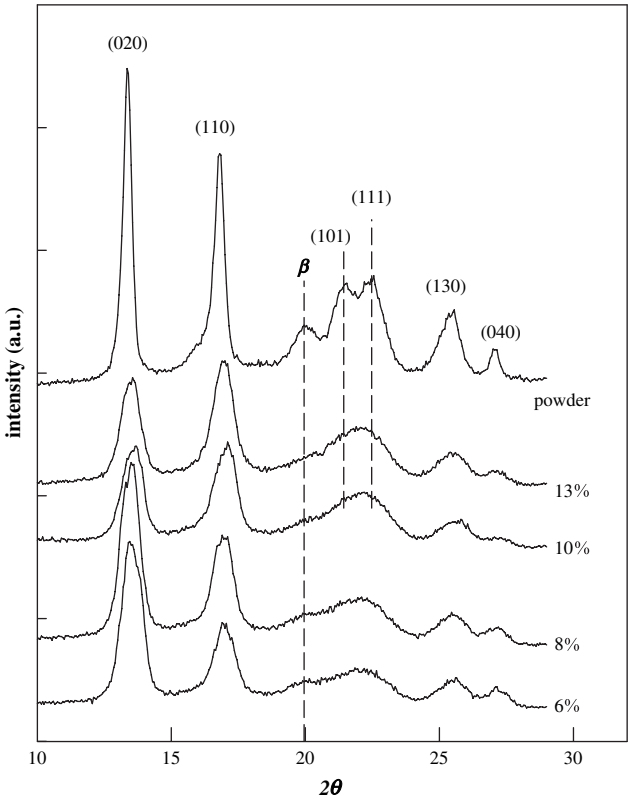

Fig. 8. WAXD intensity profiles of the PHB powder sample and PHB fiber mats electrospun from solutions with different concentrations. The diffraction planes associated with the helical α crystalline form are indexed. The small hump at 2θ–20° indicates the presence of zigzag β crystalline form.

Table 3
Properties of fiber mats electrospun from solutions with different PHB concentrations

PHB conc. (wt.%)	T_m (°C)	ϕ^{DSC}	A_{1721}/A_{1453}	A_{1228}/A_{1453}
6	173.2	0.62	14.06	2.40
8	173.6	0.61	17.46	2.08
10	173.6	0.65	18.75	2.35
13	174.0	0.63	19.55	2.38
As-received powder	172.5	0.64	–	–

α-form lamellae readily proceeds, and the interlaced chains between the crystalline lamellae are further elongated during jet whipping to develop the β-form crystals with zigzag formation. Judging from the broad diffraction peaks (Fig. 8), the size of α-form crystals formed in the electrospun PHB fibers is smaller than that of the as-received powder samples. Within the electrospun fibers, moreover, the relative population of (020) crystal plane to (110) plane is reversed as the PHB concentration is increased from 6 to 13 wt.%, suggesting plausibly that different preferred routes for the crystal growth are followed. DSC heating traces on our as-spun PHB fiber mats show that no cold crystallization takes place, and the measured melting temperature and crystallinity fraction are 173.2–174.0 °C and 0.61–0.65 (Table 3), respectively, regardless of the solution concentrations. For the powder samples, the measured T_m and ϕ^{DSC} are 172.5 °C and 0.63, respectively. Also tabulated in Table 3 are the absorbance ratios of A_{1228}/A_{1453} and A_{1721}/A_{1453} obtained by FTIR for estimating the fiber crystallinity. It is found that the A_{1228}/A_{1453} ratio remains relatively constant and independent of the PHB solution content, and is consistent with the DSC results. In contrast, a slight increase in the A_{1721}/A_{1453} ratio is observed with increasing PHB concentration owing possibly to the somewhat difficult de-convolution of the heavily overlapping peaks in this wavenumber region (1650–1800 cm^{-1}). In other words, the ratio of A_{1228}/A_{1453} seems to be more appropriate to represent the relative crystallinity of PHB fibers in consideration of its absence of required peak de-convolution.

4. Conclusion

Under an applied electric field setup by the electrodes, the diameter of pendent drops protruding from a capillary with a diameter of D_o is reduced to d_j associated with the electrified jet ejecting from the Taylor cone, and goes further down to d_f after solvent evaporation during the whipping process. The calculated diameter reduction ratios of D_o/d_j and d_j/d_f imply that major chain orientation occurs in the straight jet region, especially at the jet entrance region in the vicinity of Taylor-cone apex where an accelerating flow field is developed [25]. Based on our FEA calculation, the electric field beneath the needle-end is independent of the tip-to-collector distance, and its strength is decreased with the distance from the needle-end in a power law manner. We conclude that the diameter of electrospun fibers is determined by two quantities, i.e., the d_j and the electric field at the region where jet whipping takes place. In other words, an electrified straight jet with a smaller d_j and shorter length is favored in producing a finer electrospun fiber since it experiences a larger electric field for jet whipping. The present PHB/[CF/DMF] system also served as a model solution to reveal the viscosity dependence of jet/fiber morphologies since its surface tension and conductivity remained unchanged in the semi-dilute entangled regime. Our results showed that both d_j and d_f followed a power law relation with the viscosity: d_j–$\eta_o^{0.06}$, and d_f–$\eta_o^{0.39}$.

Acknowledgments

The authors are grateful to the National Science Council of Taiwan (ROC) for the research grant (NSC94-2216-E-006-004) that supported this work. Financial support from the "Landmark Program" of the NCKU top University Project (#B0147) to purchase the FTIR Spectrum 100 is acknowledged with gratitude.

References

[1] Li D, Xia Y. Adv Mater 2004;16:1151.
[2] Ramakrishna S, Kazutoshi F, Teo WE, Lim TC, Ma Z. An introduction to nanofibers. Singapore: World Scientific Co., Pte. Ltd; 2005.
[3] Reneker DH, Fong H. Polymeric nanofibers. In: ACS symposium series 918. Washington, DC: American Chemical Society; 2006.
[4] Teo WE, Ramakrishna S. Nanotechnology 2006;17:R89.
[5] Reneker DH, Yarin AL, Zussman E, Xu H. In: Aref H, Van Der Giessen E, editors. Advances in applied mechanics, vol. 41. London: Elsevier/Academic Press; 2007. p. 43–195.
[6] Greiner A, Wendorff JH. Angew Chem Int Ed 2007;46:5670.
[7] Baumgarten PK. J Colloid Interf Sci 1971;36:71.
[8] Fong H, Chun I, Reneker DH. Polymer 1999;40:4585.
[9] Casper CL, Stephens JS, Tassi NG, Chase DB, Rabolt JF. Macromolecules 2004;37:573.
[10] Wang C, Chien HS, Hsu CH, Wang YC, Wang CT, Lu HA. Macromolecules 2007;40:7973.
[11] Sombatmankhong K, Suwantong O, Waleetorncheepsawat S, Supaphol P. J Polym Sci Polym Phys 2006;44:2923.
[12] Ishii D, Lee WK, Kasuya KI, Iwata T. J Biotechnol 2007;132:318.
[13] Kim GM, Michler GH, Henning S, Radusch HJ, Wutzler A. J Appl Polym Sci 2007;103:1860.
[14] Choi JS, Lee SW, Jeong L, Bae SH, Min BC, Youk JH, et al. Int J Biol Macromol 2004;34:249.
[15] Ito Y, Hasuda H, Kamitakahara M, Ohtsuki C, Tanihara M, Kang IK, et al. J Biosci Bioeng 2005;100:43.
[16] Cheng ML, Lin CC, Su HL, Chen PY, Sun YM. Polymer 2008;49:546.
[17] Furuhashi Y, Imamura Y, Jikihara Y, Yamane H. Polymer 2004;45:5703.
[18] Tanaka T, Yabe T, Teramachi S, Iwata T. Polym Degrad Stab 2007;92:1016.
[19] Furuhashi Y, Ito H, Kikutani T, Yamamoto T, Kimizu M, Cakmak M. J Polym Sci Polym Phys 1998;36:2471.
[20] Terada M, Marchessault RH. Int J Biol Macromol 1999;25:207.
[21] Marchessault RH, Okamura K, Su CI. Macromolecules 1970;3:735.
[22] Graessley WW. Viscoelastic and flow in polymeric fluids in physical properties of polymers. 3rd ed. Cambridge, UK; 2004.
[23] Theron SA, Zussman E, Yarin AL. Polymer 2004;45:2017.
[24] Larsen G, Spretz R, Velarde-Ortiz R. Adv Mater 2004;16:166.
[25] Wang C, Hsu CH, Lin JH. Macromolecules 2006;39:7662.
[26] Sato H, Murakami R, Padermshoke A, Hirose F, Senda K, Noda I, et al. Macromolecules 2004;37:7203.
[27] Xu J, Guo BH, Yang R, Wu Q, Chen GQ, Zhang ZM. Polymer 2002;43:6893.
[28] Barham PJ, Keller A, Otun EL, Holmes PA. J Mater Sci 1984;19:2781.
[29] Colby RH, Fetters LJ, Funk WG, Graessley WW. Macromolecules 1991;24:3873.
[30] Desbrieres J. Biomacromolecules 2002;3:342.
[31] Son WK, Youk JH, Lee TS, Park WH. Polymer 2004;45:2959.
[32] McKee MG, Elkins CL, Long TE. Polymer 2004;45:8705.
[33] Zussman E, Yarin AL, Bazilevsky AV, Avrahami R, Feldman M. Adv Mater 2006;18:348.
[34] McKee MG, Wilkes GL, Colby RH, Long TE. Macromolecules 2004;37:1760.
[35] Shenoy SL, Bates WD, Frisch HL, Wnek GE. Polymer 2005;46:3372.
[36] Cloupeau M, Prunet-Foch B. J Electrostatic 1989;22:135.
[37] Han T, Yarin AL, Reneker DH. Polymer 2008;49:1651.
[38] Yarin AL, Koombhongse S, Reneker DH. J Appl Phys 2001;89:3018.
[39] Gañán-Calvo AM. Phys Rev Lett 1997;79:217.
[40] Helgeson ME, Wagner NJ. AIChE J 2007;53:51.
[41] Gupta PG, Elkins C, Long TE, Wilkes GL. Polymer 2005;46:4799.
[42] Daga VK, Helgeson ME, Wagner NJ. J Polym Sci Polym Phys 2006;44:1608.
[43] Dayal QP, Liu J, Kumar S, Kyu T. Macromolecules 2007;40:7689.
[44] Reneker DH, Kataphinan W, Theron A, Zussman E, Yarin AL. Polymer 2002;41:6785.
[45] Yokouchi M, Chatani Y, Tadokoro H, Teranishi K, Tani H. Polymer 1973;14:267.
[46] Orts WJ, Marchessault RH, Bluhm TL, Hamer GK. Macromolecules 1990;23:5368.